

Calculation of optimal fiber radius and whispering-gallery mode spectra for a fiber-coupled microsphere

Michael J. Humphrey, Elijah Dale, A.T. Rosenberger*, D.K. Bandy

Department of Physics, Oklahoma State University, 145 Physical Sciences, Stillwater, OK 74078-3072, United States

Received 14 October 2005; received in revised form 13 October 2006; accepted 13 October 2006

Abstract

Coupled-mode theory is used to numerically calculate the coupling coefficients between the modes of a tapered fiber and those of a fused-silica microsphere. In the visible and near-infrared wavelength ranges, typical tapered fibers are multimode. To maximize the photon tunneling from the fundamental fiber mode to the microsphere whispering-gallery mode and to minimize the tunneling from the sphere to higher-order fiber modes, the optimal fiber radius is found to be somewhat smaller than that for phase matching. Also calculated are whispering-gallery mode spectra that take into account the eccentricity of the microsphere and the fact that in an experiment the tapered fiber is not necessarily perfectly aligned with the equatorial plane of the microsphere.

© 2006 Elsevier B.V. All rights reserved.

PACS: 42.81.Qb; 42.60.Da

Keywords: Fiber waveguides, couplers, and arrays; Resonators, cavities, amplifiers, arrays, and rings

1. Introduction

In a dielectric microsphere, light in the form of a whispering-gallery mode (WGM) propagates around the equator, spatially confined to a narrow region near the sphere's surface, guided by total internal reflection. Fused-silica microspheres have extremely low WGM losses that allow them to be used as high- Q microresonators [1,2]. Such microresonators have been shown to have potential use in many areas, including cavity quantum electrodynamics [3], laser stabilization [4], microlasers [5–8], nonlinear optics [9–11], and evanescent-wave sensing [12,13]. The utility of a microsphere resonator can be limited because of the morphology dependence of the resonant frequencies of the WGMs – i.e., the resonant frequencies are fixed by the geometry of the sphere and thus not easily tunable. However, experimental advances in compression tuning [14–16] and locking of microsphere WGM resonances

[15,16] has improved these conditions by providing for tuning over a greater range with faster response. Many of these optical systems employ the technique of evanescently coupling light into and out of the WGMs of the microspheres via photon tunneling from and to modes of tapered optical fibers (see Fig. 1). Although widely used, this technique requires consideration of experimental effects associated with less than ideal conditions in the coupling process. Presented here are calculations that detail the effects of varying the size of the tapered-fiber radius and that explore the WGM spectra associated with the non-ideal aspects of an experiment.

Tapering a fiber, by any of several methods, introduces some interesting effects that must be considered. The fiber configuration often used is the bitaper. A bitaper consists of a non-tapered portion of the fiber at the first end, into which the laser light is launched. This is followed by a taper transition region where the radius of the fiber decreases with distance. The portion of the fiber after the transition is known as the taper. This is followed by a second taper transition region of increasing fiber radius and ends with

* Corresponding author. Tel.: +1 405 744 6742; fax: +1 405 744 6811.
E-mail address: atr@okstate.edu (A.T. Rosenberger).

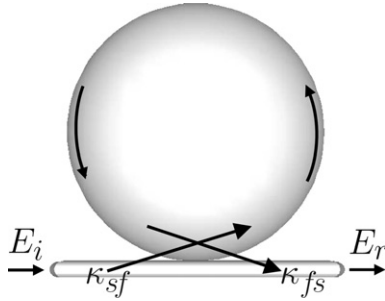


Fig. 1. Microsphere evanescently coupled to a tapered fiber. In this diagram E_i and E_r indicate the incident and reflected electric fields as in standard ring cavity notation. The κ 's refer to the coupling coefficients between the fiber and microsphere modes. The arrows indicate the direction of propagation in the fiber taper and microsphere.

another non-tapered portion. The non-tapered portion of a single-mode fiber is designed to support only the fundamental mode; hence the small size of the core relative to the transmission wavelength and the low index contrast between the core and the cladding. However, in the tapered portion of the fiber, the light is guided by the cladding–air interface and thus the tapered fiber can support multiple modes. In an ideal adiabatic taper transition, the taper angle is small enough so that the fundamental HE_{11} mode can be considered unperturbed as it evolves from being core guided to cladding guided. Within a non-ideal or non-adiabatic taper transition, the cladding guided HE_{11} mode couples to higher-order fiber modes of the same symmetry. The next higher-order fiber mode in the same family is the HE_{12} mode. Before coupling to the microsphere, the only excited modes in the tapered portion of the fiber are these two modes, if the taper transition is sufficiently adiabatic. After coupling with the microsphere, other higher-order fiber modes may be excited. This is because the microsphere mode may couple to any mode supported by the taper. Here we demonstrate that the radius of the tapered portion of the fiber can be chosen to maximize the coupling of the fiber HE_{11} mode to the microsphere mode, while minimizing the losses incurred by the coupling of the microsphere's WGM to the higher-order fiber modes of different families. These losses result because the light in these fiber modes does not couple back into the HE_{11} mode at the transmission end of the bitaper when the second taper transition is adiabatic. Early arguments [17,18] assumed that optimal coupling is accomplished by phase matching the microsphere mode to the fundamental fiber mode. Although this still seems to be the prevalent view [19–21], in this work we show that optimal coupling is actually accomplished by tapering the fiber to a smaller radius than that for phase matching.

Our calculation of the spectra for WGMs of different radial order q (number of radial intensity maxima) and polar order $l - |m|$ (one less than the number of intensity maxima in “latitude”) includes non-ideal factors that are present under experimental conditions. In practice, the microsphere usually has an eccentricity. This eccentricity

removes the frequency degeneracy of the modes of different polar order. Also, the fact that the tapered fiber may not be exactly aligned with the equatorial plane of the microsphere increases the number of WGMs to which the fiber may couple. With perfect alignment, only the even polar order (symmetric) modes of the microsphere are excited. With imperfect alignment, the odd polar order (antisymmetric) modes are also excited.

The method used for calculating the coupling coefficients is outlined in Section 2. Calculations of optimal fiber radii are presented in Section 3. WGM spectra calculations are discussed in Section 4, and Section 5 summarizes the results.

2. Calculation of coupling coefficients

Coupled-mode theory that is formulated for evanescent coupling between a tapered optical fiber and a microsphere can be used to calculate the probability of transmission (i.e. tunneling) of a photon from a fiber mode to a microsphere mode, or *vice versa*. This theory has been previously used to derive approximate formulae for predicting the coupling phenomena from tapered fibers to the high- Q WGMs of microsphere resonators [22]. The derivations were based on previous work [23] using the weak-coupling approximation [24]. The work that we present here advances these calculations by taking into account the vectorial nature of the fields as in Ref. [25]; specifically, both the transverse and longitudinal components are considered. The fiber–microsphere system can be considered analogous to a ring cavity with a partially reflecting mirror. In this analogy, what we are calculating is the mirror transmission T , which is related to the fiber–microsphere field coupling coefficient $\tilde{\kappa}$ by $T \cong |\tilde{\kappa}|^2$.

There are two factors critically important in determining the amount of fiber–microsphere field coupling: the amount of overlap of the fiber modes with the sphere modes and the phase-matching between them. This is true whether the coupling is for light entering the microsphere, i.e., fiber-to-microsphere coupling (FMC), or for light exiting the microsphere, i.e., microsphere-to-fiber coupling (MFC). The coupling strength for FMC at a point z in the direction of propagation is given by the overlap integral [25]

$$\kappa_{sf}(z) = \frac{\omega\epsilon_0}{4} (n_s^2 - n_o^2) N_f N_s \int \int_{A_s} (\mathbf{E}_f^t \cdot \mathbf{E}_s^{t*} + E_f^z E_s^{z*}) dx dy, \quad (1)$$

where $\kappa_{sf}(z)$ is the coupling coefficient, n_s and n_o are the indices of refraction of the microsphere and air, and $\mathbf{E}_{f(s)}^t$ and $E_{f(s)}^z$ are the transverse and longitudinal components of the electric field of the fiber (microsphere). The coupling coefficient is a smooth function of z because of the curvature of the microsphere's surface. The curvature affects the amplitudes of the projections of the microsphere's field components into the fiber's coordinate system and the size of the spatial gap between the fiber and the sphere. N_f and

N_s are factors that normalize the power of the fiber and microsphere modes. They are calculated from

$$1 = \frac{1}{2} N_{f(s)}^2 \sqrt{\frac{\epsilon_0}{\mu_0}} \iint n_{f(s)}(x, y) |\mathbf{E}_{f(s)}|^2 dx dy. \quad (2)$$

This means that $\kappa_{sf}(z)$ is in units of m^{-1} . Because the WGM is unidirectional and occupies a region very near to the surface of the microsphere, we can treat the microsphere as a waveguide. The fact that it is a resonator is because of round-trip boundary conditions, which are independent of the coupling tunneling probability. In coupled-mode theory, the integration takes place over the cross section of the guide into which the light is being coupled. Therefore, the integration for FMC in Eq. (1) is performed over the cross-sectional area of the microsphere A_s , where the x and y -axes are transverse to the direction of propagation. For the relevant case of weak coupling (i.e. the coupling coefficients are small compared to the propagation constants or effective wavenumbers), the total coupling including phase-matching effects is found to be [23]

$$\tilde{\kappa}_{sf} = \int_{-\infty}^{\infty} \kappa_{sf}(z) e^{i(\beta_f - \beta_s)z} dz, \quad (3)$$

where β_f and β_s are the propagation constants of the fiber and microsphere modes, respectively. The fiber and microsphere touch at $z = 0$. Because of the curvature of the sphere, the effective length in z over which coupling takes place is small compared to the microsphere radius. The validity of Eq. (3) is supported by the fact that the calculated coupling tunneling probability, $|\tilde{\kappa}|^2$, is never greater than a few percent. Thus by substituting Eq. (1) into Eq. (3), FMC can be summarized by the overlap integral

$$\tilde{\kappa}_{sf} = \frac{\omega \epsilon_0}{4} (n_s^2 - n_o^2) N_f N_s \times \iiint_{V_s} (\mathbf{E}_f^t \cdot \mathbf{E}_s^{t*} + E_f^z E_s^{z*}) e^{i\Delta\beta z} dx dy dz, \quad (4)$$

where $\tilde{\kappa}_{sf}$ is the total coupling coefficient, and $\Delta\beta = \beta_f - \beta_s$ is the difference in propagation constants of the two modes. Integration for FMC is then conveniently performed over the volume of the microsphere V_s . For MFC, the subscripts f and s are interchanged in Eq. (4), and the range of integration of the overlap integral is over the volume of the fiber. In this study, results are obtained by performing a full three-dimensional numerical integration, assuming that the fiber and microsphere are placed in contact with each other at one point.

3. Optimal fiber radius

The optimal fiber radius is determined by calculating the coupling coefficient between the fiber and microsphere. Under conditions defined below for FMC, the coupling coefficients for the HE_{11} and HE_{12} fiber modes are calculated with respect to the coupling to either of the microsphere transverse electric (TE) or transverse magnetic (TM) WGMs as a function of the radius of the tapered

fiber. Any maxima that develop in each curve would reflect an optimal coupling for a given radius of the microsphere. These optimal coupling conditions can be explained in terms of the two factors identified in Section 2: the amount of overlap of the respective fiber–microsphere modes and the phase matching between them.

Fig. 2 shows the dependence of FMC on the radius of the taper with respect to both the HE_{11} and HE_{12} fiber modes, for a given microsphere size. In Fig. 2, the most important feature is evident in the coupling of the fiber HE_{11} mode to the TE or TM fundamental modes ($q = 1$, $l = |m|$) of the microsphere: the strongest couplings occur at maxima where the fiber radius is smaller than the radius for perfect phase matching between modes (indicated by lines A and B). The reason for the increase in the coupling strength for smaller radii than for the phase-matching point is seen directly from Eq. (4). As the taper radius is decreased (from the point of phase matching), the spatial overlap of the fields is increased. At the same time, the increasing phase mismatch reduces the coupling between the two modes. The increasing effect of the spatial overlap is stronger than the decreasing effect of the phase mismatch until the radius that maximizes the coupling coefficient is reached. For radii below this, the decreasing effect of the phase mismatch is stronger than the increasing effect of the spatial overlap. The asymmetry of the profiles in Fig. 2 is a result of the fact that the fiber modes change more with radius as the radius decreases. (Note. It is not valid to interpret the optimal coupling condition as being the condition that restores phase matching between the fiber and microsphere modes once they are placed in near proximity to one another. When in contact, the presence of each waveguide only increases the effective index experienced by the mode of the other waveguide by less than one

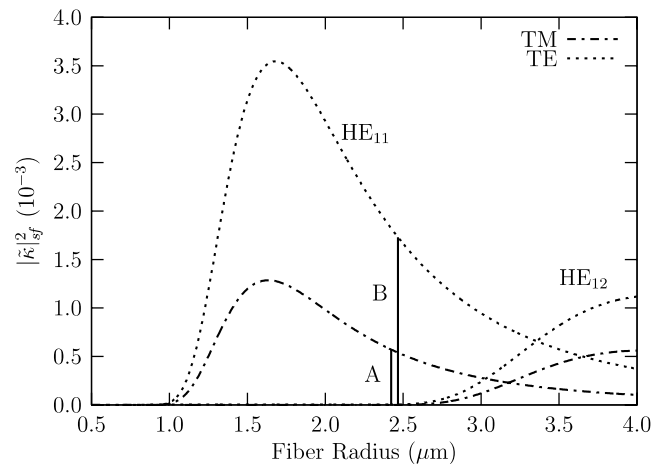


Fig. 2. Optimal fiber radius. (FMC for fiber and microsphere in contact, $R_{\text{sphere}} = 300 \mu\text{m}$, $\lambda = 1550 \text{ nm}$, $n_s = n_f = 1.44$, $n_o = 1.00$, $q = 1$, $l = |m| = 0$.) The lines that peak for fiber radii of about $1.6 \mu\text{m}$ are for HE_{11} coupling and lines that peak for fiber radii of about $4.0 \mu\text{m}$ are for HE_{12} coupling. The vertical lines A and B indicate where the fiber HE_{11} mode is perfectly phase matched to the fundamental microsphere TM and TE modes, respectively.

hundredth of a *per cent*. The effective index of the fiber HE_{11} mode is one and a half *per cent* less for the fiber size that produces maximal coupling than for the size that produces phase matching with the microsphere mode.)

The HE_{11} and HE_{12} modes have their strongest coupling at different taper radii. Thus, by changing the taper radius, the coupling can be selected to be primarily from either one of these modes. Similarly, at a certain radius of the taper, the coupling can be chosen to be from a superposition of the two modes. See, for example, a radius in the range of 3.0–3.5 μm in Fig. 2. Both the HE_{11} mode and the HE_{12} mode couple less strongly to the microsphere TM modes than to the microsphere TE modes. This can be explained by the nature of the microsphere TE and TM modes themselves. The electric fields of the TE modes in the coupling region are tangent to the surfaces of the microsphere and fiber. The electric fields of the TM modes are primarily perpendicular to the surfaces and are discontinuous, but the TM modes also have nonzero longitudinal field components. Fig. 2 indicates that the contributions of the transverse and longitudinal components of the fields in Eq. (4) are opposing for both the HE_{11} and the HE_{12} modes because the coupling is stronger to the TE mode than to the TM mode.

In the previous discussion, only the fiber-to-microsphere mode coupling is examined. It is appropriate, however, to consider also the microsphere-to-fiber light coupling. In the latter process, there are more taper modes available for the microsphere WGMs to excite. The coupling strengths are calculated for all modes with propagation constants between those of the HE_{11} and HE_{12} modes as functions of the radius as in FMC. The results for MFC are shown in Fig. 3. The maximal coupling strengths indicated in Fig. 3 are different from those indicated in Fig. 2. This is because the tunneling probability between two waveguides is the same in both tunneling directions only when the two modes are phase matched [25]. This is analogous to the unequal probabilities for particle tunneling back and forth between two potential wells with unequal energy levels. For comparison, the fundamental microsphere TE and TM modes are selected to be individually coupled to the taper modes (see Fig. 3(a) and (b), respectively). In both cases, the strongest coupling strength at a small taper radius is for the HE_{11} mode. As the taper radius is increased, the next maximal coupling coefficients correspond to the TE_{01} (in Fig. 3(a)) and the TM_{01} (in Fig. 3(b)) with the HE_{21} taper mode in third place. A superposition of the TE_{01} , HE_{21} , and TM_{01} fiber modes forms the LP_{11} mode in the linearly polarized (LP) approximation. The reason that coupling from the TE microsphere modes to the TE_{01} mode is noticeably stronger than to the HE_{21} mode is that all of the TE_{01} 's power is in the transverse direction. The strength of the coupling from the TM microsphere mode to the HE_{21} and TM_{01} modes is almost identical because both of these fiber modes have both transverse and longitudinal components. Note in Fig. 3(a) and (b) that if a radius is selected at $\sim 2.5 \mu\text{m}$

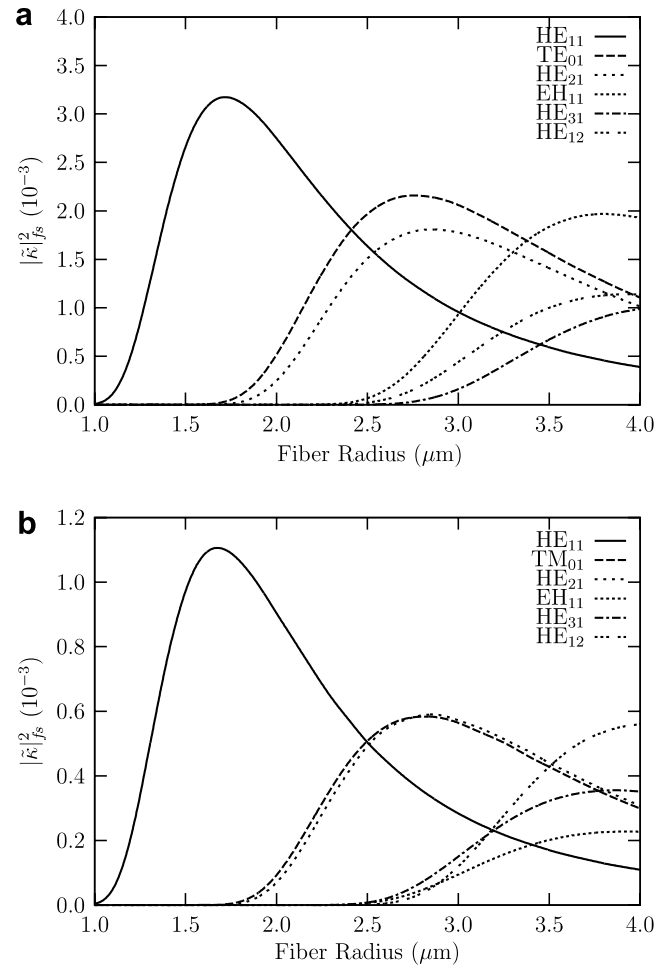


Fig. 3. Losses to higher-order fiber modes. (MFC for fiber and microsphere in contact, $R_{\text{sphere}} = 300 \mu\text{m}$, $\lambda = 1550 \text{ nm}$, $n_s = n_f = 1.44$, $n_o = 1.00$, $q = 1$, $l - |m| = 0$.) The modes are listed in order of decreasing propagation constant. (a) Coupling from fundamental microsphere TE mode to higher-order fiber modes. (b) Coupling from fundamental microsphere TM mode to higher-order fiber modes.

(the HE_{11} phase-matched point indicated by lines A and B in Fig. 2), the strength of the coupling to the fiber TE_{01} , HE_{21} , and TM_{01} modes is very close to that of the HE_{11} mode.

With MFC, coupling to the higher-order modes (HE_{12} , HE_{31} , and EH_{11}) of the taper occurs at larger radii (3.0–4.0 μm) and exhibits different behavior with respect to the TE and TM modes of the microsphere. In the case of TE mode coupling (Fig. 3(a)), the third highest maximum coupling strength corresponds to the EH_{11} taper mode, followed by the HE_{12} and the HE_{31} . There are interesting differences in the case of the TM mode coupling to the higher-order fiber modes (Fig. 3(b)). First, note that the third highest maximum coupling strength corresponds to the HE_{12} taper mode, followed by the HE_{31} and the EH_{11} , a sequence that is completely different from TE mode coupling (Fig. 3(a)). Second, not only is the order of the coupling strength between these modes different from the TE mode coupling, but there is also a functional

crossing of coupling strengths for these three modes within the radius range of ~ 2.5 – $3.2 \mu\text{m}$.

The coupling is strongly dependent on both microsphere size and wavelength. The dependence of FMC on microsphere size for the HE_{11} and HE_{12} modes is shown in Fig. 4(a) and (b), respectively. The figures show that as the microsphere size is decreased the optimal taper radius decreases while the coupling strength increases. The optimal taper radius decreases because the propagation constant of the microsphere decreases with smaller sizes. The taper size must then be decreased for better phase matching. The coupling coefficients increase with decreasing microsphere size because the spatial overlap of the fields is increased. The dependence of FMC on wavelength for the HE_{11} and HE_{12} modes is shown in Fig. 5(a) and (b), respectively. These figures show that as the wavelength increases from 800 nm to 1900 nm the optimal taper radius increases, as does the coupling strength. The coupling strength increases because the evanescent portions of the modes increase. The optimal taper radius increases because the taper size must be increased to maintain a small amount of phase mismatch with the WGM. This is because increasing the wavelength causes

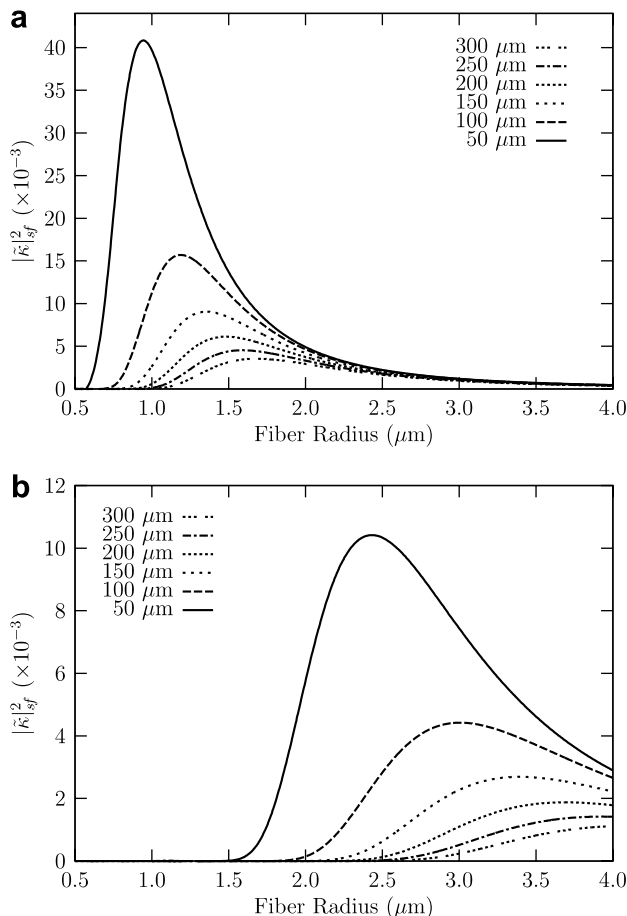


Fig. 4. Optimal fiber radius for different microsphere radii. (Fiber and microsphere in contact, $\lambda = 1550 \text{ nm}$, $n_s = n_f = 1.44$, $n_o = 1.00$, $q = 1$, $l - |m| = 0$.)

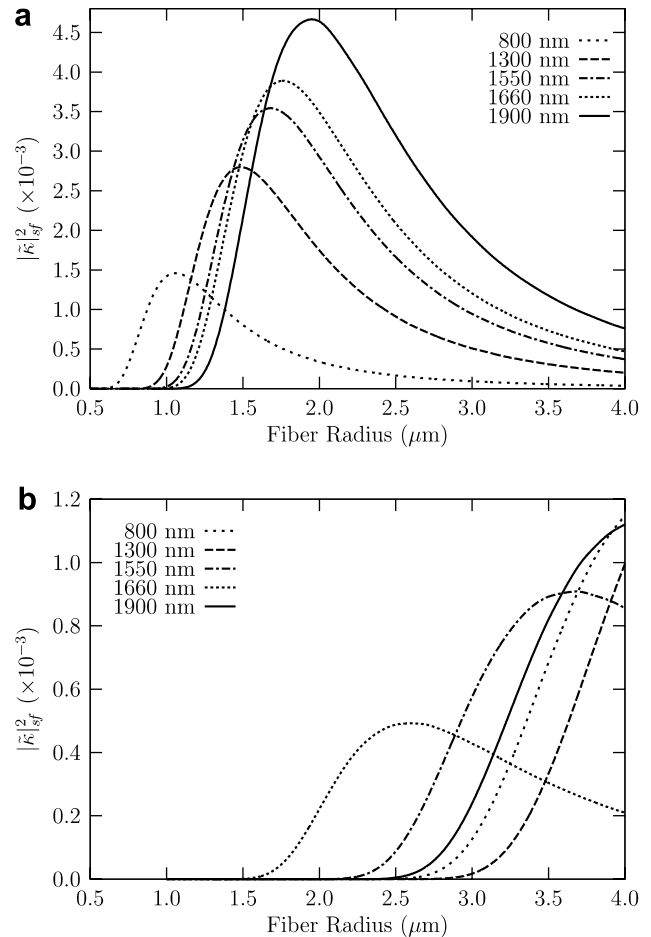


Fig. 5. Optimal fiber radius for different wavelengths. (Fiber and microsphere in contact, $R_{\text{sphere}} = 300 \mu\text{m}$, $n_s = n_f = 1.44$, $n_o = 1.00$, $q = 1$, $l - |m| = 0$.)

a larger decrease in the propagation constant for the fiber mode than that for the microsphere mode, as the wavelength of the light is closer to the size of the fiber than to the size of the microsphere.

Although the actual coupling is strongly dependent on microsphere size and wavelength, the ratio of the optimal fiber radius to the phase-matched fiber radius is only weakly dependent on the size of the microsphere and the wavelength. For all cases in Figs. 4 and 5, the optimal radius is roughly 70% of the phase-matched radius. Similarly, in all cases the coupling strength is roughly doubled by using the optimal taper radius rather than the phase-matched radius.

The coupling to higher-order microsphere modes is also of interest because it is unlikely that the fundamental mode is excited in an experiment. Calculations indicate that for higher radial order modes the optimal taper radius is smaller, while the coupling strength at the optimal taper radius is larger. For example, for a microsphere of radius $300 \mu\text{m}$ and wavelength 1550 nm , the maximum coupling from the HE_{11} fiber mode to the fundamental TE microsphere mode is $|\tilde{k}|^2 = 3.6 \times 10^{-3}$ with a taper radius of $1.68 \mu\text{m}$, as seen in Fig. 2. The maximum coupling to a mode of fundamen-

tal polar order and third radial order ($q = 3$) is calculated to be $|\tilde{\kappa}|^2 = 5.6 \times 10^{-3}$ with a fiber radius of $1.48 \mu\text{m}$. This is a result of the higher radial order modes having lower propagation constants and larger evanescent fractions. Coupling to higher polar order modes results in weaker coupling, but only a very small change in the optimal taper radius. For example, the maximum coupling to a mode of fundamental radial order and second polar order ($l - |m| = 2$) is calculated to be $|\tilde{\kappa}|^2 = 1.4 \times 10^{-3}$ with a taper radius of $1.68 \mu\text{m}$. The coupling is weaker because the higher-order microsphere modes have a wider polar distribution, resulting in less spatial overlap with the fiber mode. The optimal taper radius is shifted very little because the difference in propagation constants is small between modes of different polar order.

The discussion of optimal taper radius is not complete without some remarks about the polarization of the modes. In FMC, the orientation of the HE_{11} and HE_{12} fiber fields is used to choose whether the coupling is to TE or TM microsphere modes. For coupling to TE microsphere modes, the orientation is chosen such that the transverse electric fields are tangent to the surfaces of the fiber and microsphere within the interaction region. For coupling to TM modes, the orientation is chosen so that the electric fields are perpendicular to the surfaces in the interaction region. In MFC, the orientations are chosen in the same manner. However, coupling is possible for modes whose electric field orientations are in-between being perfectly perpendicular and tangent to the surfaces in the interaction region. In fact, none of the modes can be oriented completely as in either of these situations. This is because the modes of the taper are not perfectly linearly polarized. Although the orientation of the fields can be used to cause the coupling to be primarily to microsphere TE or TM modes, the orientation can never entirely eliminate coupling to either of these families of modes. Calculations, not shown here, indicate that the coupling to the orthogonal polarization is two and a half orders of magnitude weaker than the coupling to the primary polarization.

4. WGM spectra

The microsphere WGM spectra are calculated by numerically integrating the field overlap integral in Eq. (4) under less than ideal conditions. The condition of a fiber taper offset from the equatorial plane of the microsphere is considered. In this configuration, non-zero overlap is possible between the fiber mode and odd polar order (antisymmetric) modes of the microsphere. Thus, these modes couple in addition to even polar order (symmetric) modes that couple when the alignment is perfect. Recall that in a perfectly spherical microsphere the polar modes are frequency degenerate. This degeneracy is broken by introducing an eccentricity to the microsphere. The frequencies of WGMs in such microspheres are given by [4,26]

$$v_{qim}^i \cong \delta \left[l + \frac{1}{2} + a_q \left(\frac{l + 1/2}{2} \right)^{1/3} - \Delta^i \pm \varepsilon^2 \left(\frac{l - |m|}{2} \right) \right], \quad (5)$$

where i denotes TE or TM, $\delta = c/2\pi R_s n_s$ is the microsphere's nominal free-spectral range, where R_s is the equatorial radius of the microsphere. a_q is the absolute value of the q th zero of the Airy function and the different forms of Δ^i give the polarization shift of the WGM frequencies: $\Delta^{\text{TE}} = n(n^2 - 1)^{-1/2}$, and $\Delta^{\text{TM}} = n^{-1}(n^2 - 1)^{-1/2}$, where $n = n_s/n_o$. For the last term in Eq. (5), the upper sign is used for an oblate spheroid and the lower sign for the prolate case, where the eccentricity is given in terms of the ellipsoid major and minor radii R_+ and R_- as $\varepsilon^2 = (R_+^2 - R_-^2)/R_+^2$.

In Fig. 6, the WGM wavelengths within one free-spectral range are displayed, under the condition of misalignment of the taper modes with the WGMs of the equatorial plane. The radius has been chosen to optimally couple the HE_{11} taper mode to the fundamental TE microsphere mode. The offset from the equatorial plane has been chosen to be $\theta_{\text{off}} = \pi/76$. In Fig. 6, $\varepsilon^2 \sim 0.09$, so major and minor radii differ by about 5%. The wavelengths are grouped according to different modes of radial order q . Within each grouping, modes of eight polar orders are shown (i.e., $l - |m| = 0, 1, \dots, 7$), with the polar order increasing with increasing wavelength. Some of these modes are not visible on the scale of the coupling selected in the figure because of their low coupling coefficients. It is clear that for an offset fiber, higher polar order modes can have stronger coupling than the fundamental polar order mode. In this case, the polar order modes with $l - |m| = 2$ have the strongest coupling. This is because of the choice of offset. For other offsets, different polar order modes have stronger coupling. In the case of no lateral offset, the fundamental polar order modes have the highest coupling. This is followed by weaker coupling for each successive even higher polar order mode. For clarity, only a small fraction of the actual number of modes is shown. Because

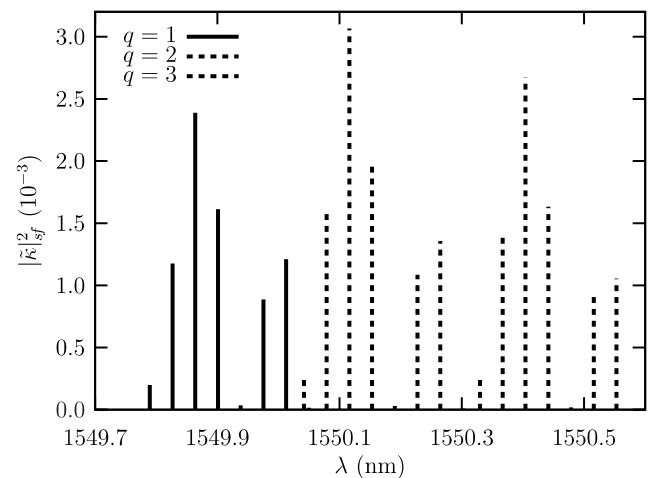


Fig. 6. WGM TE spectrum. (FMC for fiber and microsphere in contact, $R_s = 300 \mu\text{m}$, $R_f = 1.68 \mu\text{m}$, prolate with $\varepsilon = 0.29$, $\theta_{\text{off}} = \pi/76$.) For $q = 1$, $l = 1730$; for $q = 2$, $l = 1713$; for $q = 3$, $l = 1699$.

this graph is over one free-spectral range, modes of higher radial order would begin again from the left with $q = 4$. These modes continue to wrap around the plotted wavelength range. Higher polar order modes ($l - |m| > 7$) would also overlap with modes of different radial order.

5. Conclusions

The calculations of optimal fiber radii indicate that the highest coupling from a fundamental fiber mode to a fundamental microsphere mode is achieved with a fiber that has a taper radius somewhat smaller (about 30%) than that for perfect phase-matching. For a taper of this size, the coupling is about twice as strong as when phase-matched. Another advantage of using the smaller size taper is that losses to higher-order fiber modes are substantial for phase-matched sizes. Also, the calculations indicate that coupling to the microsphere TE modes is stronger than to the TM modes. This is a result of the longitudinal field overlap present when coupling into TM modes. With increasing wavelength, the optimal taper radius decreases slightly while the coupling coefficients increase. Calculations show that the optimal fiber radii are almost unchanged when the surrounding medium has a higher than unity index of refraction. For an external index of 1.33, the optimal fiber radius for the HE_{11} mode is the same, while the coupling strength is increased by almost exactly an order of magnitude.

In all of the calculations in this work, the microsphere and fiber are assumed to be in contact; if they were not, all of the coupling coefficients would be reduced. For example, coupling of 1550 nm light from the HE_{11} fiber mode to the fundamental TE microsphere mode is $|\tilde{\kappa}|^2 = 3.6 \times 10^{-3}$ when fiber and microsphere are in contact (300 μm radius sphere, see Fig. 2). For separation distances of 0.2 μm and 0.4 μm the coupling strengths are reduced to 7.2×10^{-4} and 1.4×10^{-4} , respectively. This is because of the exponential decay of the modes' evanescent fields. In addition, some of the relative coupling strengths between the modes would be different. This is because some higher-order modes have longer decay lengths than lower-order modes.

The calculation of WGM spectra under the offset taper condition shows that there are many possible modes that can be coupled within one free-spectral range of the microsphere. The calculated values of the coupling coefficients are consistent with experimental data [8,27]. For example, for the overcoupled 830 nm pump mode in Fig. 4 of Ref. [8] (300 μm radius sphere, 1.5 μm radius fiber), a value of $T = 1.5 \times 10^{-3}$ is found from the experimental throughput trace.¹ It is close to the theoretical peak value of $|\tilde{\kappa}|^2$ for 800 nm, as in Fig. 5(a), but with

$q = 2$. This is reasonable because modes of several radial orders are commonly excited in an experiment. With the fiber laterally offset from, but still parallel to the equatorial plane of the microsphere, the coupling to the fundamental polar order mode is not as strong as to some of the higher polar order modes. This is also in agreement with experimental data [27] and is a result of higher polar order modes having greater polar extent. The inclusion of eccentricity and lateral offset enables the numerical calculations to be directly compared to experimental data. All calculations are valuable both for designing experiments and interpreting the resulting data. This research is being extended to sphere-to-sphere coupling for application to coupled-resonator induced transparency and absorption theory [28] and experiments [29].

Acknowledgments

This research was supported by the Oklahoma Center for the Advancement of Science and Technology under Project Nos. AR012-064 and AR022-052, and the National Science Foundation, Award Nos. ECS-0115442 and ECS-0329924.

References

- [1] V.B. Braginsky, M.L. Gorodetsky, V.S. Ilchenko, Phys. Lett. A 137 (1989) 393.
- [2] D.W. Vernooy, V.S. Ilchenko, H. Mabuchi, E.W. Streed, H.J. Kimble, Opt. Lett. 23 (1998) 247.
- [3] D.W. Vernooy, A. Furusawa, N.P. Georgiades, V.S. Ilchenko, H.J. Kimble, Phys. Rev. A 57 (1998) R2293.
- [4] V.V. Vassiliev, V.L. Velichansky, V.S. Ilchenko, M.L. Gorodetsky, L. Hollberg, A.V. Yarovitsky, Opt. Commun. 158 (1998) 182.
- [5] V. Sandoghdar, F. Treussart, J. Hare, V. Lefèvre-Seguin, J.-M. Raimond, S. Haroche, Phys. Rev. A 54 (1996) 1777.
- [6] M. Cai, O. Painter, K.J. Vahala, P.C. Sercel, Opt. Lett. 25 (2000) 1430.
- [7] F. Lissillour, P. Féron, N. Dubreuil, P. Dupriez, M. Poulain, G.M. Stéphan, Electron. Lett. 36 (2000) 1382.
- [8] S.I. Shopova, G. Farca, A.T. Rosenberger, W.M.S. Wickramanayake, N.A. Kotov, Appl. Phys. Lett. 85 (2004) 6101.
- [9] D. Braunstein, A.M. Khazanov, G.A. Koganov, R. Shuker, Phys. Rev. A 53 (1996) 3565.
- [10] A.T. Rosenberger, in: R.B. Lal, D.O. Frazier (Eds.), Operational Characteristics and Crystal Growth of Nonlinear Optical Materials, Proceedings of SPIE, vol. 3793, 1999, p. 179.
- [11] A.N. Oraevsky, D.K. Bandy, Opt. Commun. 129 (1996) 75.
- [12] A.T. Rosenberger, J.P. Rezac, in: A.V. Kudryashov, A.H. Paxton, Laser Resonators III, Proceedings of SPIE, vol. 3930, 2000, p. 186.
- [13] A.T. Rosenberger, J.P. Rezac, in: R.P. Mariella Jr., D.V. Nicolau (Eds.), Biomedical Instrumentation Based on Micro- and Nanotechnology, Proceedings of SPIE, vol. 4265, 2001, p. 102.
- [14] V.S. Ilchenko, P.S. Volikov, V.L. Velichansky, F. Treussart, V. Lefèvre-Seguin, J.-M. Raimond, S. Haroche, Opt. Commun. 145 (1998) 86.
- [15] J.P. Rezac, A.T. Rosenberger, in: A.V. Kudryashov, A.H. Paxton (Eds.), Laser Resonators IV, Proceedings of SPIE, vol. 4270, 2001, p. 112.
- [16] J.P. Rezac, A.T. Rosenberger, Opt. Express 8 (2001) 605.
- [17] J.C. Knight, G. Cheung, F. Jacques, T.A. Birks, Opt. Lett. 25 (1997) 1129.
- [18] M.L. Gorodetsky, V.S. Ilchenko, J. Opt. Soc. Am. B 16 (1999) 147.

¹ The dip depth is $M = 0.45$ and the dip width is $\Delta\nu = 30$ MHz. Because this is an overcoupled mode, the dip depth corresponds to a coupling loss to intrinsic loss ratio of $X = 6.6$. The dip width indicates a quality factor of $Q = 1.2 \times 10^7$. The transmission is then found to be ($n_s = 1.44$) $T = \frac{4\pi^2 n_s R_s}{\lambda Q(1+\frac{1}{X})} = 1.5 \times 10^{-3}$.

- [19] O.J. Painter, D.W. Vernooy, K.J. Vahala, Modulators incorporating multi-layer dispersion-engineered waveguides, US Patent Application: 20050135721 (November 15, 2004).
- [20] O.J. Painter, D.W. Vernooy, K.J. Vahala, Fabrication of multi-layer dispersion-engineered waveguides, US Patent Application: 20050135764 (November 16, 2004).
- [21] S.M. Spillane, T.J. Kippenberg, O.J. Painter, K.J. Vahala, *Phys. Rev. Lett.* 91 (2003) 043902.
- [22] B.E. Little, J.-P. Laine, H.A. Haus, *J. Lightwave Technol.* 17 (1999) 704.
- [23] B.E. Little, S.T. Chu, H.A. Haus, J. Foresi, J.-P. Laine, *J. Lightwave Technol.* 15 (1997) 998.
- [24] A.W. Snyder, J.D. Love, *Optical Waveguide Theory*, Chapman and Hall Ltd., 1983, p. 556.
- [25] S.-L. Chuang, *J. Lightwave Technol.* LT-5 (1987) 5.
- [26] S. Schiller, R.L. Byer, *Opt. Lett.* 16 (1991) 1138.
- [27] J.P. Rezac, Properties and applications of whispering-gallery mode resonances in fused silica microspheres, Ph.D. thesis, Oklahoma State University 2002.
- [28] D.D. Smith, H. Chang, K.A. Fuller, A.T. Rosenberger, R.W. Boyd, *Phys. Rev. A* 69 (2004) 063804.
- [29] A. Naweed, G. Farca, S.I. Shopova, A.T. Rosenberger, *Phys. Rev. A* 71 (2005) 043804.